ECCOMAS Congress 2016
VII European Congress on Computational Methods in Applied Sciences and Engineering
M. Papadrakakis, V. Papadopoulos, G. Stefanou, V. Plevris (eds.)
Crete Island, Greece, 5–10 June 2016

A LOW DIFFUSIVE APPROACH FOR TWO PHASE FLOWS

A. Beccantini

CEA Saclay, Université Paris-Saclay,
Laboratoire de Dynamique des Structures, DEN/DM2S/SEMT/DYN,
F-91191 Gif-sur-Yvette Cedex
e-mail: alberto.beccantini@cea.fr

Keywords: Compressible multifluid flows, Discrete Equation Method, Upwind Downwind-Controlled Splitting, Anti-diffusive scheme, Tangent of hyperbola interface capturing

Abstract. *We present a work realized in the framework of the R&D program on the Hydrogen combustion of the I3P Project "accidents graves parc actuel". It is a sequel to recent publications (Tang et al., 2014) where high-order and low diffusive approaches (e.g. a multi-dimensional anti-diffusive approach) and an original Upwind Downwind-Controlled Splitting method (UDCS) were combined with the 1D and multi-dimensional formulations of DEM (Discrete Equation Method, Abgrall and Saurel 2003) and RDEM (Reactive Discrete Equation Method, Le Métayer et al., 2005).*

On one hand, the UDCS limited second-order method has already been combined with the explicit two-step Runge-Kutta scheme for time discretization and represents a significant improvement of the previous limited second-order RDEM approach in terms of robustness (it is now implemented in the fast dynamic fluid-structure interaction code EUROPLEXUS to compute reacting flows in 3D large geometries like the containment of a nuclear power plant).

On the other hand, as observed on the final 2D combustion problem presented in (Tang et al., 2014), it was necessary to improve the approach used to compute the normal vector at the flame interface so as to avoid that the computation of this normal spoils the accuracy improvement brought by the anti-diffusive UDCS/RDEM.

In this work a modification of the anti-diffusive approach has been realized using a hyperbolic tangent approximation of the phase function (or color function) to correctly compute its gradient and then normals to the flame interface. On one hand, numerical experiments have shown that this approach is more accurate than the limited second-order method. On the other hand, the problem of flame wrinkling (which also affects the limited second-order method) is not completely solved (as expected since numerical diffusion of the new approach is less important than in the limited second-order method), but it can be reduced if gradients are computed not directly to the phase function but on a field obtained by solving a diffusion problem having the phase function as initial condition.

1 Introduction

This work is a sequel to recent publications [1, 2, 3, 4] where high-order and low diffusive approaches (e.g. a multi-dimensional anti-diffusive approach) and an original Upwind Downwind-Controlled Splitting method (UDCS) were combined with the 1D and multi-dimensional formulations of DEM [5] and RDEM [6, 7]. First, the method was successfully developed in 1D for computing inert interfaces (e.g. impermeable water-gas shock tube problem) and flame interfaces (e.g. Chapman-Jouguet deflagration and strong detonation wave) with excellent robustness and accuracy properties. Secondly, it has been successfully extended to the multi-dimensional case for the modeling of multi-fluid flows on unstructured grids.

The limited second-order UDCS method has already been combined with the explicit two-step Runge-Kutta scheme for time discretization. This allow us to work with large enough CFL numbers when using a limited second-order reconstruction on all primitive variables (achieving quasi second-order accuracy in space and time). As shown in [4], this approach represents a significant improvement of the classical second-order RDEM approach in terms of robustness and is now implemented in the fast dynamic fluid-structure interaction code EUROPLEXUS [8] to compute reacting flows in 3D large geometries (e.g. the containment of a nuclear power plant). Details can be found in [9, 10, 11].

As shown in [3, 4], the anti-diffusive UDCS is much more accurate than the limited second-order UDCS. For instance, when computing a 1D flame acceleration with the latter approach, the flame region can become too large, thus weakening the precursor shock wave. On the opposite the anti-diffusive UDCS method keeps the flame region over one or two cells, thus avoiding the weakening of the precursor shock wave; however, in multi-dimensional computation, since the flame region is crisped, it is impossible to define a normal to the flame surface. For this reason we propose here a new approach, in which the the flame region is diffused over a region of fixed width; this is obtained by using the properties of the hyperbolic tangent function (tanh) to decide whether to add numerical diffusion to the antidiffusive approach. We point out that the idea of using an hyperbolic tangent function to represent a color function (or a phase function) has already been used in the THINC (tangent of hyperbola interface capturing) scheme of Xiao and coworkers, presented for the first time in [12]; some improvements on Cartesian grids are proposed in [13, 14, 15]; and extensions to unstructured meshes can be found in [16, 17]. However our approach, which is also devoted for computation in unstructured meshes, is quite different and does not require the reconstruction of tahn: the smoothing of the color function is obtained by adding numerical diffusion to the antidiffusive approach when necessary.

2 Numerical approach

This section is organized as follows. First of all we briefly introduce the hyperbolic tangent (Section 2.1). Since the smoothing of the color function is obtained by the modification of the anti-diffusive approach, for the sake of simplicity we first present the anti-diffusive approach of Lagoutière [18] and its tanh modification in 1D, in the particular case of monotone color function (respectively in Section 2.2 and Section 2.3). Then we present the 1D general case in Section 2.4. Finally Section 2.5 is devoted to the multi-dimensional case.

2.1 The hyperbolic tangent and the smoothed color function

The hyperbolic tangent $\tanh(x/l)$, with

$$\tanh(x) = \frac{\sinh(x)}{\cosh(x)} = \frac{\frac{1}{2}(\exp(x) - \exp(-x))}{\frac{1}{2}(\exp(x) + \exp(-x))},$$

can be considered as a smoothed Heaviside function varying from -1 to 1. As shown in Figure 1, it coincides with the Heaviside function as $l \to 0$, l being a length scale which determines the smoothness of the function.

A smoothed color function α, $\alpha_{\min} < \alpha < \alpha_{\max}$ can be described by the function

$$\begin{aligned} \alpha(x, l, \alpha_{\min}, \alpha_{\max}) &= \frac{1}{2}\alpha_{\min}\left(1 - \tanh\left(\frac{x}{l}\right)\right) + \frac{1}{2}\alpha_{\max}\left(1 + \tanh\left(\frac{x}{l}\right)\right) \\ &= \frac{\alpha_{\min} + \alpha_{\max}}{2} + \frac{\alpha_{\max} - \alpha_{\min}}{2}\tanh\left(\frac{x}{l}\right) \end{aligned} \tag{1}$$

The reciprocal function of the color function $x(\phi)$ is

$$x(\phi) = l\ \tanh^{-1}\left(\frac{\phi - \frac{\alpha_{\min}+\alpha_{\max}}{2}}{\frac{\alpha_{\max}-\alpha_{\min}}{2}}\right), \quad \alpha_{\min} < \phi < \alpha_{\max}.$$

Figure 2 represents the color function α (equation (1)) in the particular case $\alpha_{\min} = 0.1$, $\alpha_{\max} = 0.9$ ($l = 1$ and $l = 0.1$).

2.2 The 1D anti-diffusive approach for a monotone color function

Let us illustrate form a qualitative point of view how the anti-diffusive approach works on the equation

$$\frac{\partial \alpha}{\partial t} + D\frac{\partial \alpha}{\partial x} = 0$$

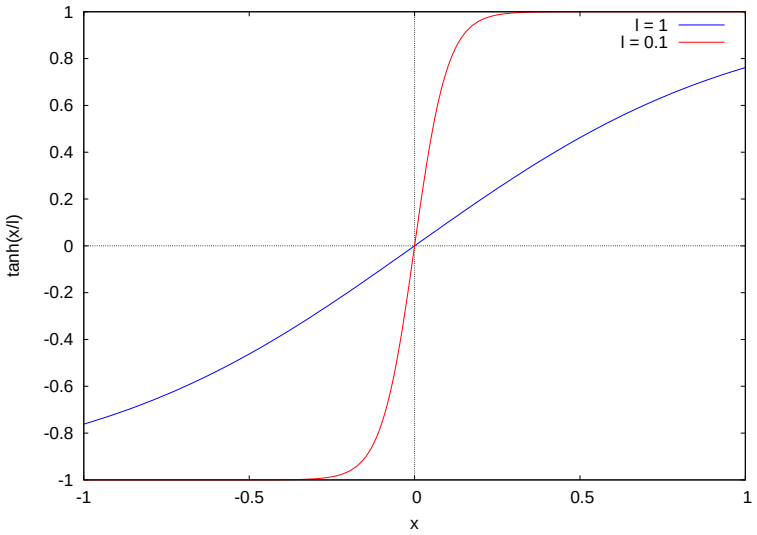

Figure 1: The hyperbolic tangent $\tanh(x/l)$.

with $D > 0$ and α monotone decreasing function

$$\frac{\partial \alpha}{\partial x} \leq 0,$$

(see for instance Figure3). With a conservative finite volume discretisation explicit in time we can write in the i-th cell

$$\frac{\alpha_i^{n+1} - \alpha_i^n}{\Delta t} = \frac{D}{\Delta x} \left(\alpha_{i-1/2}^n - \alpha_{i+1/2}^n \right), \tag{2}$$

α_i being value inside the i-th cell and $\alpha_{i\pm 1/2}$ intercell values (see Figure 4).
According to the monotone condition for α, we suppose $\alpha_{i-1}^n \geq \alpha_i^n \geq \alpha_{i+1}^n$.

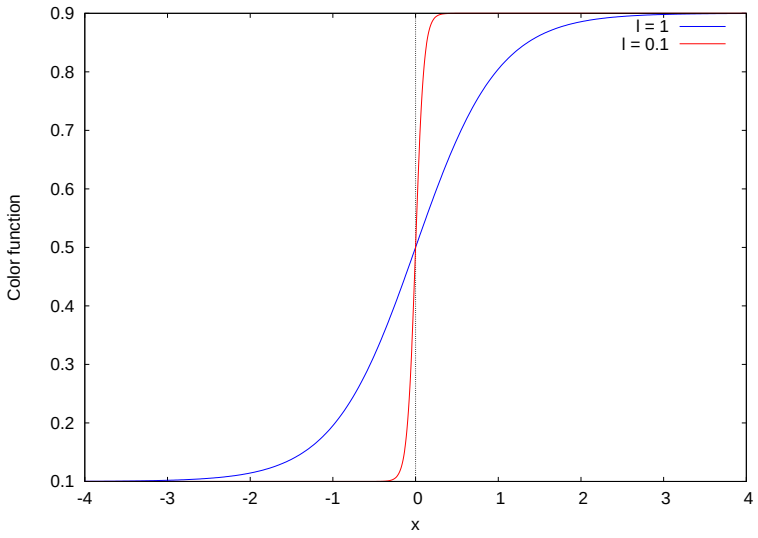

Figure 2: The color function (1) when $\alpha_{\min} = 0.1$, $\alpha_{\max} = 0.9$ ($l = 1$ and $l = 0.1$).

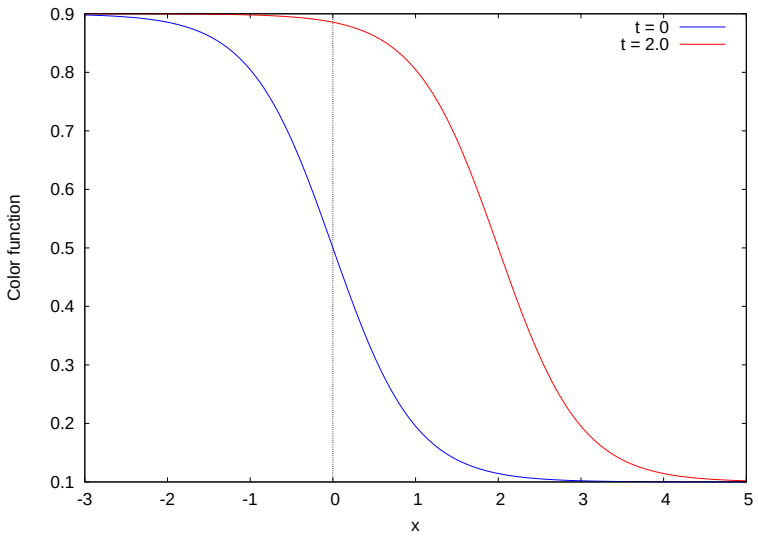

Figure 3: Example of translation of a monotone decreasing color function $\alpha(x)$ with speed 1, namely plot of $\alpha(x - t)$ with $t = 0$ and $t = 2$.

The choice of the intercell value $\alpha_{i+1/2}$ depends on the approach we use.

- $\alpha^n_{i+1/2} = \alpha^n_i$ corresponds to the **upwind scheme** (the speed D being positive), first order accurate and conditionally stable, which diffuses the Heaviside function.
- $\alpha^n_{i+1/2} = \alpha^n_{i+1}$ corresponds to the **downwind scheme**, first order accurate and unconditionally unstable, which "anti-diffuses" the Heaviside function.
- The purpose of the **controlled anti-diffusive scheme** is the combination of both approaches to prevent the diffusion of the Heaviside function. We look for $\alpha^n_{i+1/2}$ such that
$$\alpha^n_{i+1/2} \in (\alpha^n_{i+1}, \alpha^n_i)$$
More in particular we look for the closest value to the downwind one which does not create a new extremum, namely **we look for the minimum value of $\alpha^n_{i+1/2}$ which provides the maximum value of α^{n+1}_i with**
$$\alpha^{n+1}_i \leq M^n_i = \max\left(\alpha^n_i, \alpha^n_{i-1}\right) = \alpha^n_{i-1}. \tag{3}$$

From equation (2) we can write
$$\alpha^n_{i+1/2} = \alpha^n_{i-1/2} - \frac{\Delta x}{D\Delta t}\left(\alpha^{n+1}_i - \alpha^n_i\right).$$
In order to avoid a condition which couples all the intercell faces, we take for $\alpha^n_{i-1/2}$ its most conservative value, the one which maximizes α^{n+1}_i, namely we suppose that $\alpha^n_{i-1/2} = M^n_i$. It follows that condition (3) is satisfied if $\alpha^n_{i+1/2} \geq b^n_i$ with
$$\begin{aligned} b^n_i &= M^n_i - \frac{\Delta x}{D\Delta t}\left(M^n_i - \alpha^n_i\right) \\ &= \alpha^n_i - \left(\frac{\Delta x}{D\Delta t} - 1\right)\left(M^n_i - \alpha^n_i\right) \end{aligned} \tag{4}$$
independently from the choice of $\alpha^n_{i-1/2}$ (indeed we have supposed that it assumes its worst value for condition (3)).
b^n_i is lower than the upwind value (α^n_i) providing that a CFL condition is respected. At the end we choose
$$\alpha^n_{i+1/2} = \max(\alpha^n_{i+1}, b^n_i).$$
In this way $\alpha^n_{i+1/2} \in (\alpha^n_{i+1}, \alpha^n_i)$; namely its value is between the upwind and is the closest to the downwind one which does not create new extrema.

From a mathematical point of view one can show that using this scheme the 1D solution of Heaviside function presents zero, one or two intermediate regions at each time step, i.e. as the time increases the solution is not numerically diffused.

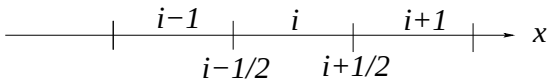

Figure 4: Conservative finite volume discretisation. x axis. Indexes $i-1$, i, $i+1$ refer to cell value. Indexes $i-1/2$, and $i+1/2$ refer to intercell values.

2.3 The tanh modification for a monotone color function

As in Section 2.2, we present the approach in the case

$$\frac{\partial \alpha}{\partial x} \leq 0,$$

and $\alpha_{i-1}^n \geq \alpha_i^n \geq \alpha_{i+1}^n$.
We suppose that in the i-th cell the color function has the shape

$$\alpha_{\tanh}\left(x - x_i\right) = \frac{1}{2} - \frac{1}{2}\tanh\left(\frac{\beta(x - x_i)}{\Delta x_i} + \tilde{x_i}\right)$$

where Δx_i is the cell dimension, β is a parameter which controls the steepness of $\alpha_{\tanh}$ (the characteristic length l is $\Delta x_i/\beta$), $\tilde{x_i}$ is a parameter we have to determine. Instead of using a condition over the integral, as in the THINC approach, we prefer considering a condition over the value. Namely we compute $\tilde{x_i}$ such that

$$\alpha_{\tanh}\left(0\right) = \alpha_i^n$$

i.e.

$$\tilde{x_i} = \tanh^{-1}\left(1 - 2\alpha_i^n\right), \quad 0 < \alpha_i^n < 1.$$

Once determined $\tilde{x_i}$, since β is given, we increase the numerical diffusion of the anti-diffusive approach by imposing a constraint on the downwind-closest value for $\alpha_{i+1/2}^n$, namely we require that

$$\alpha_{i+1/2}^n > \alpha_{\tanh}(\underbrace{x_{i+1/2} - x_i}_{0.5\Delta x}). \tag{5}$$

We define

$$\tilde{\tilde{b_i^n}} = \max(\alpha_{i+1}^n, \alpha_{\tanh}(0.5\Delta x))$$

and we want now that

$$\alpha_{i+1/2}^n \in (\tilde{\tilde{b_i^n}}, \alpha_i^n)$$

which is more restrictive than $\alpha_{i+1/2}^n \in (\alpha_i^{n+1}, \alpha_i^n)$.
Finally, conditions (4) and (5) are satisfied if

$$\alpha_{i+1/2}^n = \max(\tilde{\tilde{b_i^n}}, b_i^n).$$

where b_i^n is defined via equation (4).

The following properties hold.

- Since $\tilde{\tilde{b_i^n}} \geq \alpha_i^{n+1}$, the scheme is more diffusive than the anti-diffusive approach presented in Section 2.2.
- If the tanh restriction is not so important (i.e. $\alpha_{\tanh}(0.5\Delta x) \leq \alpha_i^{n+1}$, which implies $\tilde{\tilde{b_i^n}} = \alpha_i^{n+1}$), the scheme degenerates to the anti-diffusive approach.

2.4 The tanh modification in the 1D general case

First of all, let us present the general formula for the anti-diffusive scheme. We define

$$\begin{aligned} m_i^n &= \min\left(\alpha_{i-1}^n, \alpha_i^n\right) \\ M_i^n &= \max\left(\alpha_{i-1}^n, \alpha_i^n\right). \end{aligned}$$

We suppose that speeds $D_{i-1/2} \geq 0$, $D_{i+1/2} > 0$.
We want to find intercell boundaries values for α such that

$$m_i^n \leq \alpha_i^{n+1} \leq M_i^n \tag{6}$$
$$m_{i+1}^n \leq \alpha_{i+1/2}^n \leq M_{i+1}^n \tag{7}$$

Condition (6) is satisfied if

$$\left\{ \begin{array}{rcl} M_i^n & \geq & \alpha_i^n \\ & + & \dfrac{D_{i-1/2}\Delta t}{\Delta x_i}(M_i^n - \alpha_i^n) \\ & - & \dfrac{D_{i+1/2}\Delta t}{\Delta x_i}(\alpha_{i+1/2}^n - \alpha_i^n) \\ m_i^n & \leq & \alpha_i^n \\ & + & \dfrac{D_{i-1/2}\Delta t}{\Delta x_i}(m_i^n - \alpha_i^n) \\ & + & \dfrac{D_{i+1/2}\Delta t}{\Delta x_i}(\alpha_i^n - \alpha_{i+1/2}^n) \end{array} \right.$$

or

$$\left\{ \begin{array}{rcccl} \alpha_{i+1/2}^n & \geq & b_i^n & = & \alpha_i^n \\ & & & - & \dfrac{\Delta x_i}{D_{i+1/2}\Delta t}(M_i^n - \alpha_i^n) \\ & & & + & \dfrac{D_{i-1/2}}{D_{i+1/2}}(M_i^n - \alpha_i^n) \\ \alpha_{i+1/2}^n & \leq & B_i^n & = & \alpha_i^n \\ & & & + & \dfrac{\Delta x_i}{D_{i+1/2}\Delta t}(\alpha_i^n - m_i^n) \\ & & & - & \dfrac{D_{i-1/2}}{D_{i+1/2}}(\alpha_i^n - m_i^n) \end{array} \right. \tag{8}$$

It is difficult to show that $b_i^n \leq \alpha_i \leq B_i^n$. Then we define

$$\begin{aligned} l_i &= \max(m_{i+1}^n, \min(b_i^n, \alpha_i^n))) \\ L_i &= \min(M_{i+1}^n, \max(B_i^n, \alpha_i^n)) \end{aligned}$$

with b_i^n and B_i^n defined in (8). Since $l_i \leq \alpha_i \leq L_i$, the value of $\alpha_{i+1/2}^n$ defined as

$$\alpha_{i+1/2}^n = \begin{cases} L_i & \text{if } \alpha_{i+1}^n > L_i, \\ \alpha_{i+1}^n & \text{if } L_i \geq \alpha_{i+1}^n \geq l_i, \\ l_i & \text{if } l_i > \alpha_{i+1}^n \end{cases} \tag{9}$$

satisfies conditions (6) and (7).

We introduce numerical diffusion when the downwind value is too strong with respect to the tanh representation of α.

- If $|\alpha_{i-1}^n - \alpha_{i+1}^n| \leq 10^{-3}$ we do not modify formulae.
- If $\alpha_{i-1}^n > \alpha_{i+1}^n$ (negative centered gradient for α), then

$$\alpha_{\tanh}(x - x_i) = \frac{1}{2} - \frac{1}{2}\tanh\left(\frac{\beta(x - x_i)}{\Delta x_i} + \tilde{x}_i\right)$$

$$\tilde{x}_i = \tanh^{-1}(1 - 2\alpha_i^n), \quad 0 < \alpha_i^n < 1.$$

$$\tilde{\tilde{b}}_i^n = \max(\alpha_{i+1}^n, \alpha_{\tanh}(0.5\Delta x_i))$$

  We redefine

$$m_{i+1}^n = \min(\alpha_i^n, \tilde{\tilde{b}}_i^n)$$

  and then we proceed like in classical downwind approach.

$$\begin{aligned} l_i &= \max(m_{i+1}^n, \min(b_i^n, \alpha_i^n))) \\ L_i &= \min(M_{i+1}^n, \max(B_i^n, \alpha_i^n)) \end{aligned}$$

  where b_i^n and B_i^n are defined via formulae (8).
  Finally

$$\alpha_{i+1/2}^n = \begin{cases} L_i & \text{if } \alpha_{i+1}^n > L_i, \\ \alpha_{i+1}^n & \text{if } L_i \geq \alpha_{i+1}^n \geq l_i, \\ l_i & \text{if } l_i > \alpha_{i+1}^n \end{cases}$$

- If $\alpha_{i-1}^n < \alpha_{i+1}^n$ (positive centered gradient for α), then

$$\alpha_{\tanh}(x - x_i) = \frac{1}{2} + \frac{1}{2}\tanh\left(\frac{\beta(x - x_i)}{\Delta x_i} - \tilde{x}_i\right)$$

$$\tilde{x}_i = \tanh^{-1}(1 - 2\alpha_i^n), \quad 0 < \alpha_i^n < 1.$$

$$\tilde{\tilde{B}}_i^n = \min(\alpha_{i+1}^n, \alpha_{\tanh}(0.5\Delta x_i))$$

  We redefine

$$M_{i+1}^n = \max(\alpha_i^n, \tilde{\tilde{B}}_i^n)$$

  and then we proceed like in classical downwind approach.

$$\begin{aligned} l_i &= \max(m_{i+1}^n, \min(b_i^n, \alpha_i^n))) \\ L_i &= \min(M_{i+1}^n, \max(B_i^n, \alpha_i^n)) \end{aligned}$$

where b_i^n and B_i^n are defined via formulae (8).
Finally

$$\alpha_{i+1/2}^n = \begin{cases} L_i & \text{if } \alpha_{i+1}^n > L_i, \\ \alpha_{i+1}^n & \text{if } L_i \geq \alpha_{i+1}^n \geq l_i, \\ l_i & \text{if } l_i > \alpha_{i+1}^n \end{cases}$$

At the beginning of this section we have supposed that $D_{i-1/2} > 0$, $D_{i+1/2} > 0$. If we suppose that speed $D_{i-1/2} < 0$, $D_{i+1/2} < 0$, we proceed in the same manner. Finally, if $D_{i-1/2}.D_{i+1/2} < 0$ or if $D_{i+1/2} = 0$, we take the upwind value.

2.5 Extension to unstructured grids

The anti-diffusive approach for unstructured meshes we consider here is the one presented in [4]. Let us describe it from a qualitative point of view (see [4] for details).
As shown in Figure 5 in the i-th cell we have to distinguish between inlet and outlet interfaces, according to the scalar product of the velocity $\mathbf{D}$ and the normal vector pointing outside. At the outlet interfaces we define

$$\begin{aligned} m_{i,\text{out},j}^n &= \min\{\alpha_i^n, \alpha_{i,\text{out},j}^n\}, \\ M_{i,\text{out},j}^n &= \max\{\alpha_i^n, \alpha_{i,\text{out},j}^n\}, \\ m_{i,\text{out}}^n &= \min_j\{m_{i,\text{out},j}^n\}, \\ M_{i,\text{out}}^n &= \max_j\{M_{i,\text{out},j}^n\}, \end{aligned}$$

where index $''i, \text{out}, j''$ refers to the neighbor of the i-th cell sharing the j-th outlet interface.
At the outlet interfaces we compute the quantity $\Delta\text{up}_{i,\text{out}}^n$, which is the amount of α transmitted in the upwind case from the i-th cell to the neighbors sharing outlet interfaces. We also define the so-called downwind factor, which is the fraction of $\Delta\text{up}_{i,\text{out}}^n$ retained inside the i-th cell. A downwind factor equal to 0 means that $\Delta\text{up}_{i,\text{out}}^n$ is totally transmitted to its neighbors while a downwind factor equal to 1 means that all $\Delta\text{up}_{i,\text{out}}^n$ is totally kept inside the i-th cell.

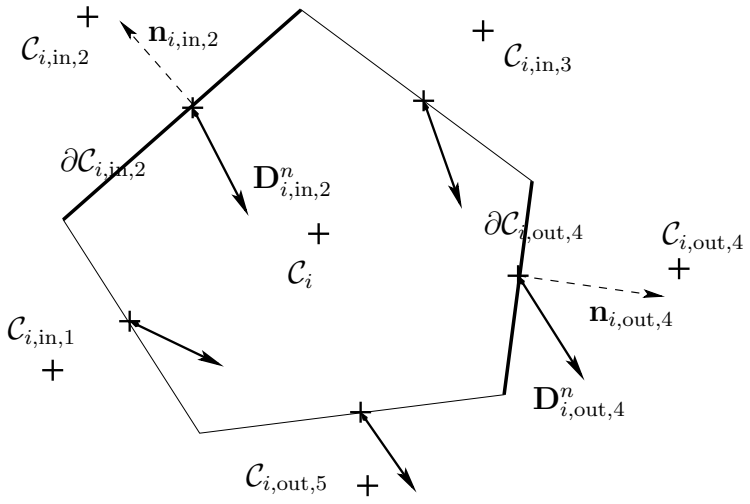

Figure 5: Two dimensional finite volume cell. Illustration for numerical resolution of the transport equation for α.

As in the 1D case, the tanh modification of the anti-diffusive scheme introduces a constraint to the downwind factor. First of all, we compute

$$\vec{n} = -\frac{\vec{\nabla}\alpha}{|\vec{\nabla}\alpha|}$$

$\vec{n}$ is directed versus the region of decreasing α. Then we suppose that, in the same direction as $\vec{n}$, α has the shape

$$\alpha_{\tanh}(s) = \frac{1}{2} - \frac{1}{2}\tanh\left(\frac{\beta s}{\Delta x_i} + \tilde{x_i}\right) \tag{10}$$

where s is the curvilinear abscissa starting from the center of the cell and

$$\tilde{x_i} = \tanh^{-1}(1 - 2\alpha_i^n).$$

We also define

$$s_{\max} = \max_{j \in \text{face}}(|\mathbf{r}_{i,j} \cdot \mathbf{n}|),$$

- If $\Delta \text{up}_{i,\text{out}}^n > 0$, the function $\alpha_{\tanh}(s)$ (which is 1 at $s = -\infty$ and 0 at $s = +\infty$) is moving in the same direction as $\vec{n}$ (namely versus positive value of s). As in 1D, we enforce that the tanh modification should limit the value of $m_{i,\text{out}}^n$. We know that

  $$\alpha_{\tanh}(s_{\max}) < \alpha_i^n.$$

  We compute

  $$\tilde{\tilde{b}}_i^n = \max\left(\alpha_{\tanh}(s_{\max}), m_{i,\text{out}}^n\right)$$

  We define

  $$\tilde{\tilde{\Lambda}}_i^n = \frac{\alpha_i^n - \tilde{\tilde{b}}_i^n}{\alpha_i^n - m_{i,\text{out}}^n}$$

  and we enforce that the downwind factor cannot be larger than $\tilde{\tilde{\Lambda}}_i^n$.

- If $\Delta \text{up}_{i,\text{out}}^n < 0$, the function $\alpha_{\tanh}(s)$ (which is 1 at $s = -\infty$ and 0 at $s = +\infty$) is moving versus the negative value of s. As in 1D, we enforce that the tanh modification should limit the value of $M_{i,\text{out}}^n$. We know that

  $$\alpha_{\tanh}(-s_{\max}) > \alpha_i^n.$$

  We compute

  $$\tilde{\tilde{B}}_i^n = \min\left(\alpha_{\tanh}(-s_{\max}), M_{i,\text{out}}^n\right)$$

  We define

  $$\tilde{\tilde{\Lambda}}_i^n = \frac{\tilde{\tilde{B}}_i^n - \alpha_i^n}{M_{i,\text{out}}^n - \alpha_i^n}$$

  and we enforce that the downwind factor cannot be larger than $\tilde{\tilde{\Lambda}}_i^n$.

Concluding, the principle of the approach is the same as in the 1D case: we introduce a constraint which involves a space scale l to increase the numerical diffusion when the space scale in the i-cell at time t^n is lower than l.

3 Numerical results

We have computed several test cases with the new approaches, which are not presented here. For instance we have verified that both approaches degenerate to the upwind one as β tends to zero ($l = \Delta x/\beta$ tends to infinity). Similarly, both approaches degenerate to the anti-diffusive one as β tends to infinity ($l = \Delta x/\beta$ tends to zero).

The first test case we present here is the propagation of a reactive shock wave. It is a good example to see the behavior of the different approaches.

The second test case is the Chapman-Jouguet deflagration shock tube previously proposed in [7]. This test case is interesting because it allows observing how the poor accuracy on the flame region can affect the accuracy on the flame-generated shock wave. Here we show that the the anti-diffusive approach with tanh modification gives results more accurate that the classical limited second order approach. In particular the number of intermediate cells does not increase with time for the former.

The third test case is a non-reactive test case and consists in the expansion of a cylindrical high-pressure region. It confirms that even in multi-dimensional computations the different approaches behave in the same manner as in 1D computations. In particular the anti-diffusive approach with tanh modification shows to be more accurate than the one involving the Barth-Jespersen reconstruction.

3.1 Moving reactive shock wave

We compute a moving reactive shock wave for a stoichiometric mixture of hydrogen-air. For the unburnt mixture

$$(\rho, v, P) = (1.069100549993681, 545.2, 139000.0)$$

SI units. For the burnt mixture

$$(\rho, v, P) = (0.1468254285125072, 829.1210885558426, 125279.9833247705)$$

SI units. The fundamental speed of the shock is $K_0 = 45.2$ m/s, which gives a visible speed of $D = (545.2 - 45.2) = 500$ m/s. Specific heats are computed as fourth degree polynomial regressions of JANAF data.

Let us now investigate the behavior of different approaches (the anti-diffusive ones with tanh present $\beta = 0.5$). We take a mesh $0 < x < 20$ m with 100 cells, a CFL equal to 0.5 and we suppose that at the beginning the reactive shock is in $x = 10$ m.

In Figure 6 we represent the volume fraction of the burnt gases α obtained using the classical first order upwind (top) and the minmod limited second-order reconstruction (bottom). As expected the result obtained with the former approach is less accurate than the one obtained with the latter one. However in both approaches the number of intermediate regions increases with time.

In Figure 7 we represent the volume fraction of the burnt gases α obtained using the anti-diffusive approach (top) the anti-diffusive approach with tanh modification. As one can see, the anti-diffusive approach presents only one intermediate region while the other one presents a number of intermediate regions (10) which does not vary with time (as expected).

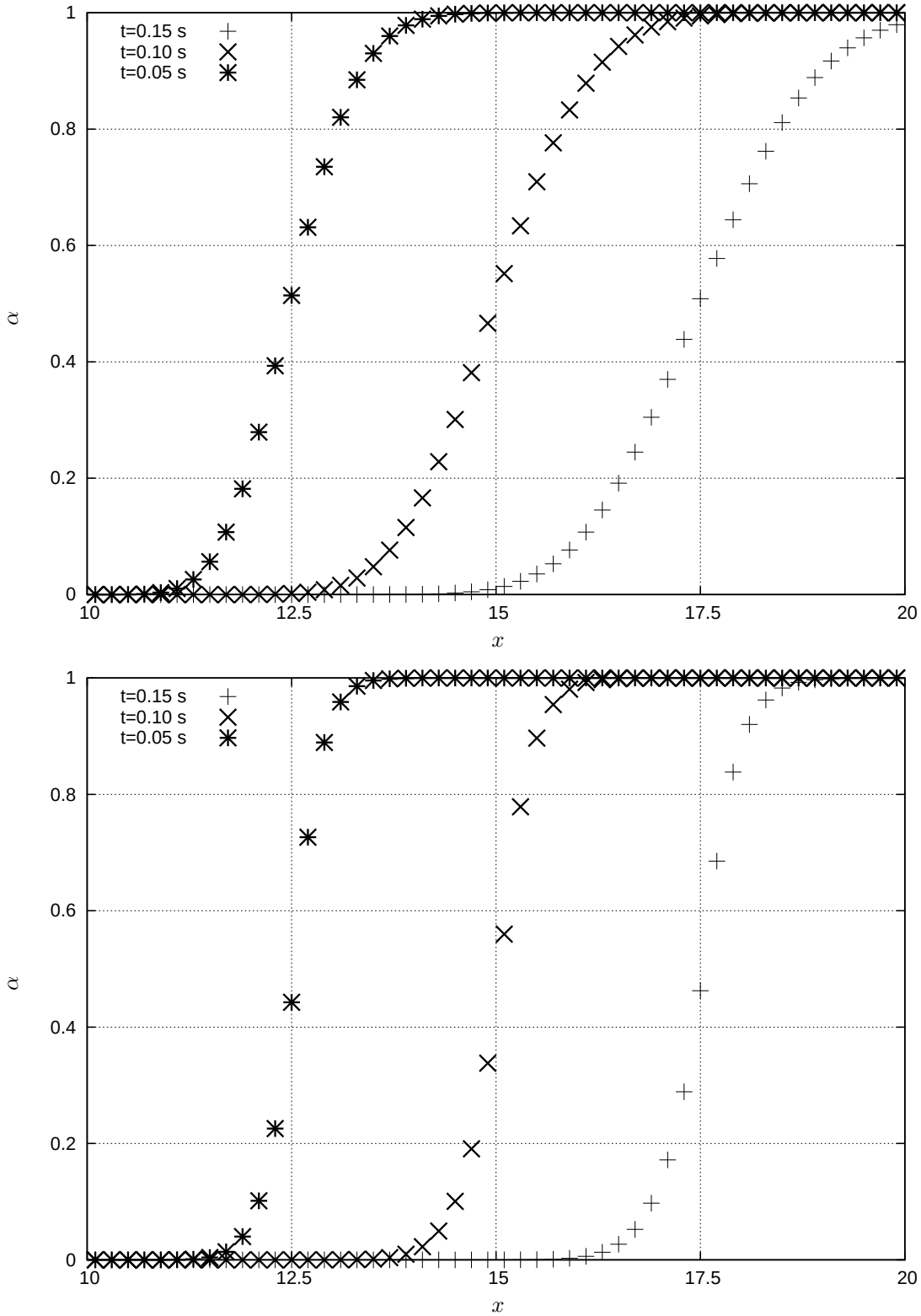

Figure 6: Propagation of a moving reactive shock wave. α, volume fraction of the burnt gases. On the top, first order upwind scheme. On the bottom, minmod limited second-order reconstruction

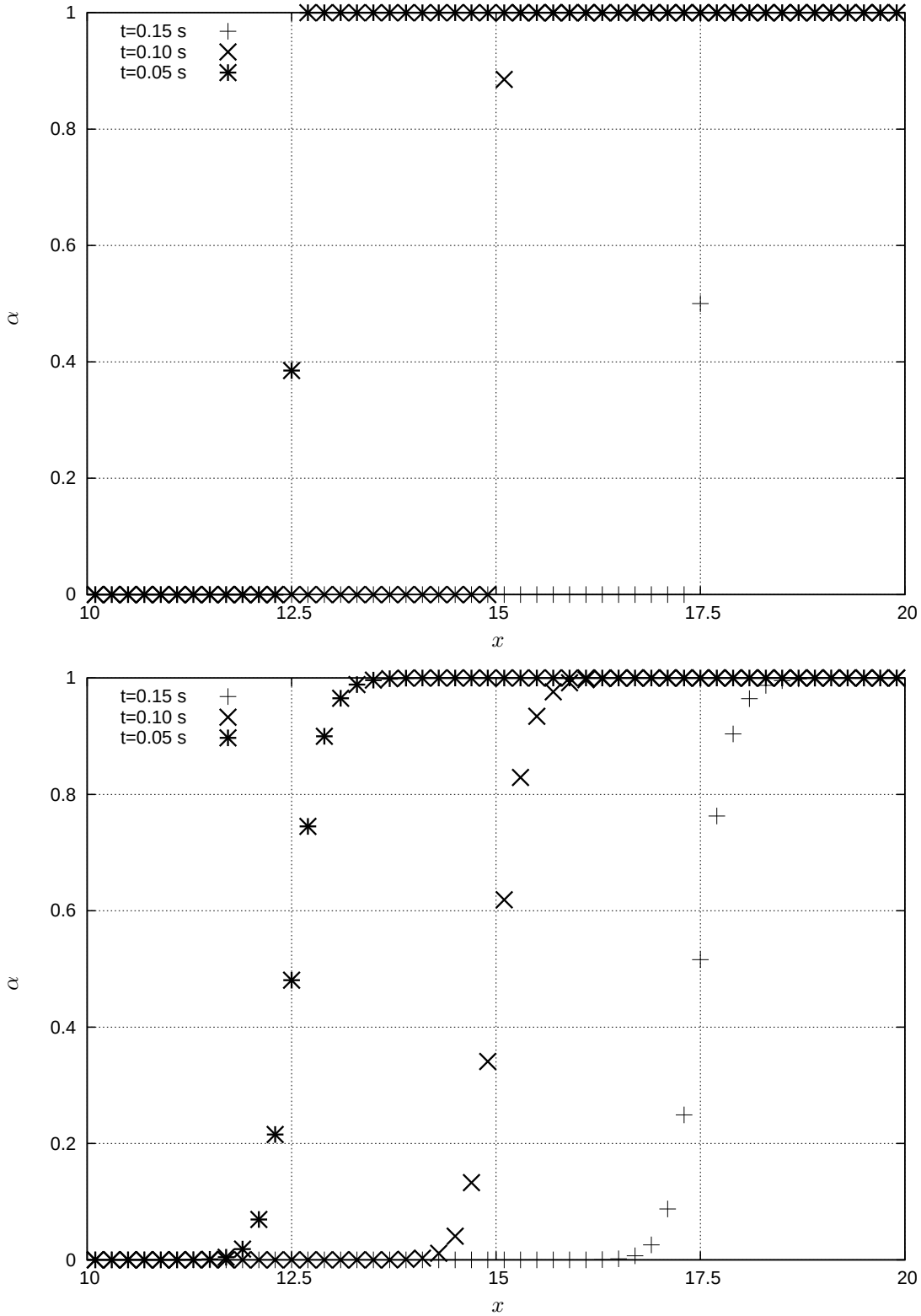

Figure 7: Propagation of a moving reactive shock wave. α, volume fraction of the burnt gases. On the bottom, anti-diffusive approach with tanh modification (case 2, limitation on the downwind-closest value).

3.2 Chapman-Jouguet deflagration shock tube

Let us consider the Chapman-Jouguet deflagration shock tube previously proposed in [7]. The 20 meter long shock tube involves on the right ($0\ \mathrm{m} \leq x \leq 10\ \mathrm{m}$) a stoichiometric mixture of hydrogen-air, with pressure and temperature equal to $1.013\ \mathrm{bar}$ and $290\ \mathrm{K}$ respectively. On the left ($-10\ \mathrm{m} \leq x \leq 0\ \mathrm{m}$), the burnt gas (due to the complete combustion of the stoichiometric mixture of hydrogen-air) is found with pressure and temperature equal to $2.013\ \mathrm{bar}$ and $2800\ \mathrm{K}$. The specific heats are computed as fourth degree polynomials of the temperature, obtained by interpolating data in JANAF tables. For the modeling and numerical reasons already explained in [5], the right part contains a very small volume of burnt gas (volume fraction is $\varepsilon = 10^{-8}$) and the left part contains a very small volume of unburnt gas (volume fraction is $\varepsilon = 10^{-8}$). The gases are initially at rest and the fundamental flame speed is set equal to $200\ \mathrm{m/s}$.

Let us now investigate the behavior of different approaches (the anti-diffusive one with tanh modification present $\beta = 0.5$). We take 1000 cells and a CFL equal to 0.75; second-order in time is achieved using an explicit Runge-Kutta scheme and we perform a minmod limited second-order reconstruction on primitive variables. Different approaches are tested on the volume fraction: minmod limited second-order reconstruction, anti-diffusive approach, anti-diffusive approach with tanh modification.

In Figure 8 we represent the burnt gas volume fraction α as function of x at different times. As usual, the minmod limited second-order reconstruction of α generates a numerical diffusion region dimension which increases with time. The anti-diffusive approach on α generates one intermediate region only. Finally the anti-diffusive approach with tanh modification generates a numerical diffusion region with about 10 cells which does not increase with time.
In Figure 9 we present the computed pressure close to the reactive front. As usual the anti-diffusive approach gives the most accurate results but the anti-diffusive approach with tanh modification also gives a correct representation of the flame region thanks to the fact that the numerical diffusion region does not increase with time.

3.3 2D Expansion of a cylindrical high-pressure high-density region

We have a quadrangular domain with 121x121 element with $\Delta x = 1$ (non-dimensional units), namely $-60.5 \leq x \leq 60.5$, $-60.5 \leq y \leq 60.5$. At the center we have a cylinder with $r = 6$ and we suppose that in the elements having their center inside this cylinder we have $P = 10^2$ and $\rho = 1.4 \cdot 10^2$ (and color function equal to 1). Outside we have $P = 1$ and $\rho = 1.4$ (and color function equal to 0). We suppose that we are dealing with a calorically perfect gas, with $\gamma = 1.4$.

Computations are realized with EUROPLEXUS using the DEMS material [8], the Euler explicit scheme for time integration, CFL = 0.25 and four different approaches:

- the upwind approach;
- UDCS combined with the Barth-Jespersen (limited second-order) reconstruction;
- UDCS combined with anti-diffusive approach;
- UDCS combined with anti-diffusive approach with tanh modification.

Because of the high-density high-pressure region, the cylindrical region expands in the low-density low-pressure region. In Figure 10 we represent the color function α at $t = 1$ and at

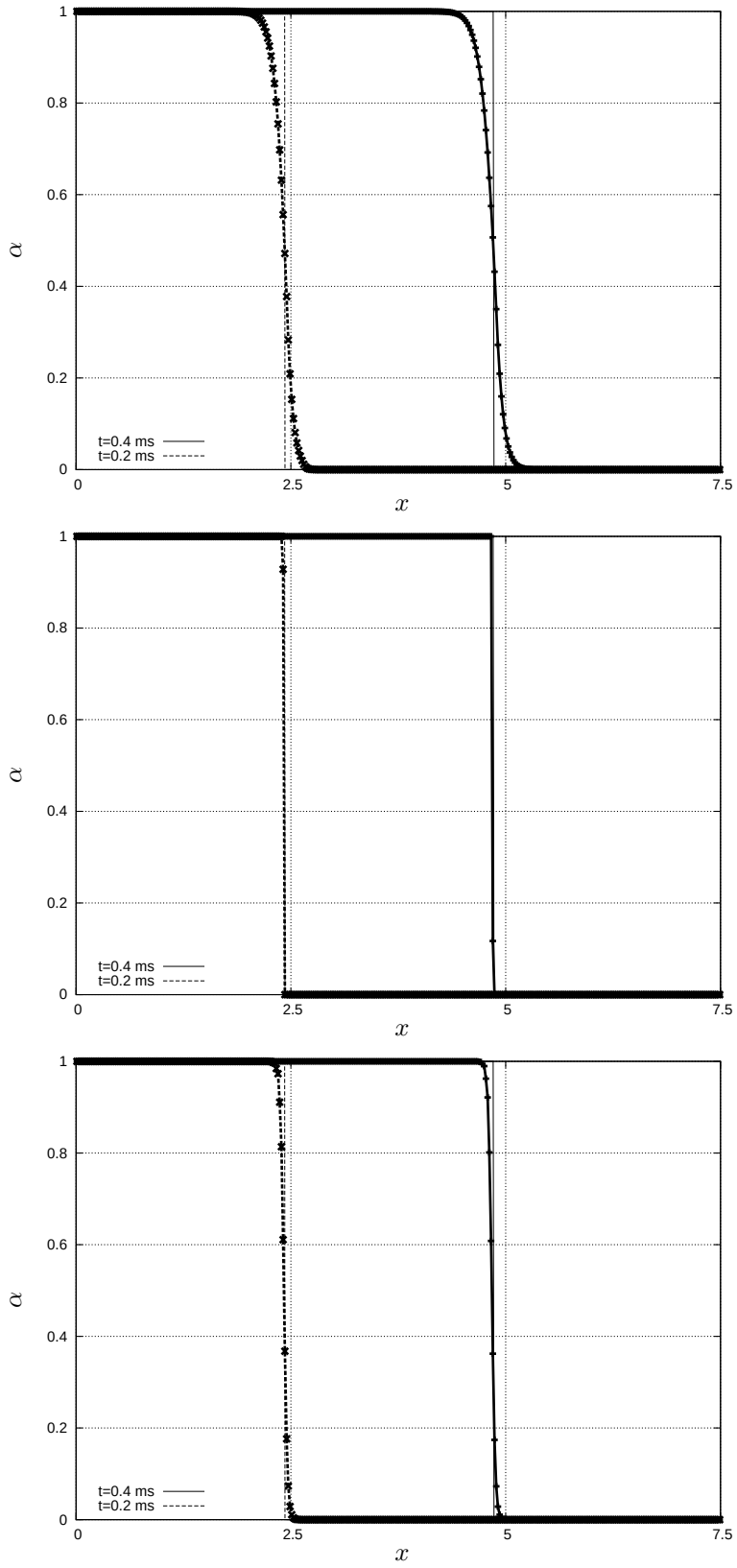

Figure 8: Chapman-Jouguet deflagration shock tube. Volume fraction of the burnt gases α as function of x (SI units). On the top, minmod limited second-order reconstruction on α. On the center anti-diffusive approach on α. On the bottom, anti-diffusive approach with tanh modification on α (the whole domain is -10 m $\leq x \leq$ 10 m).

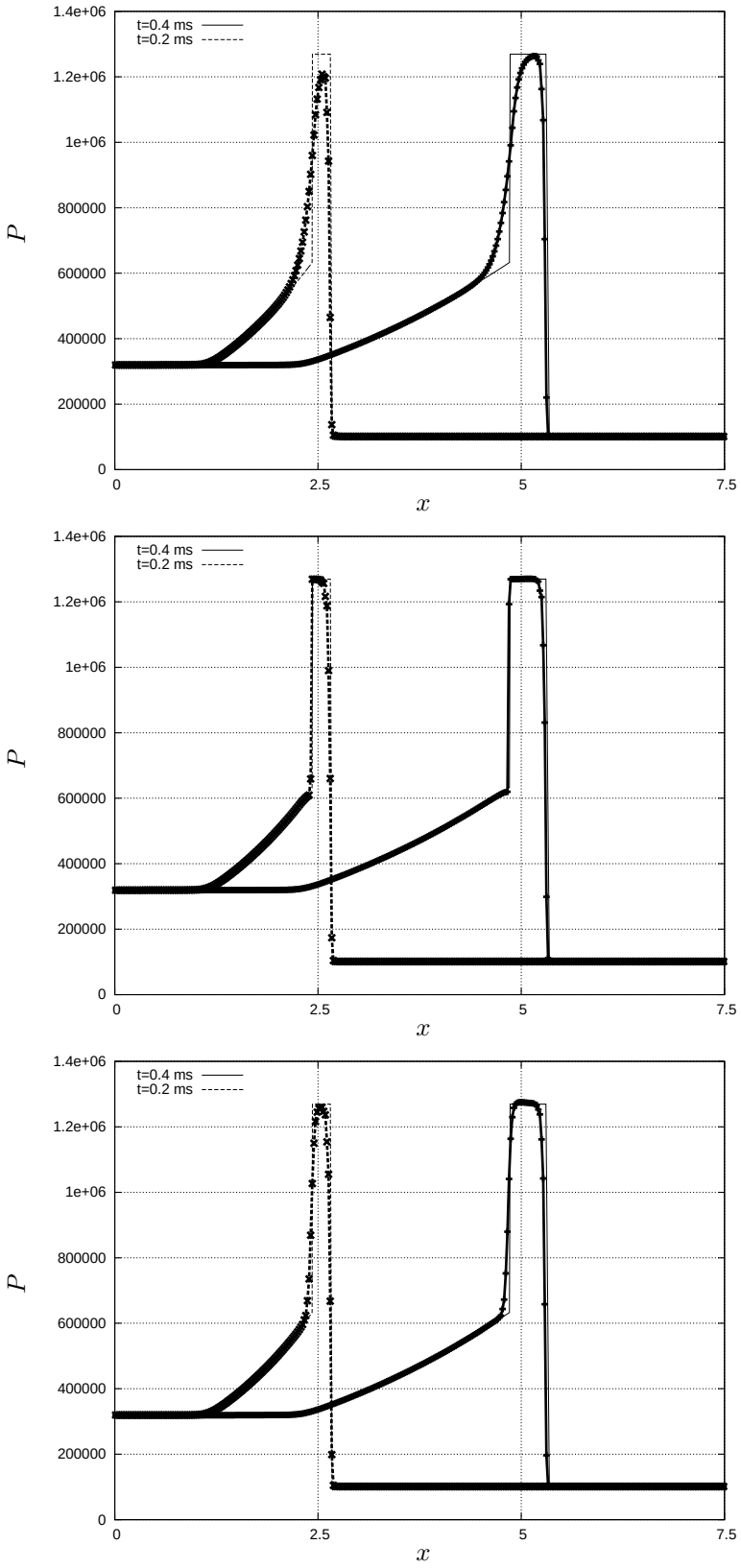

Figure 9: Chapman-Jouguet deflagration shock tube. Pressure P as function of x (SI units). On the top, minmod limited second-order reconstruction on α. On the center anti-diffusive approach on α. On the bottom, anti-diffusive approach with tanh modification on α (the whole domain is -10 m $\leq x \leq$ 10 m).

$t = 10$ obtained with the anti-diffusive approach.

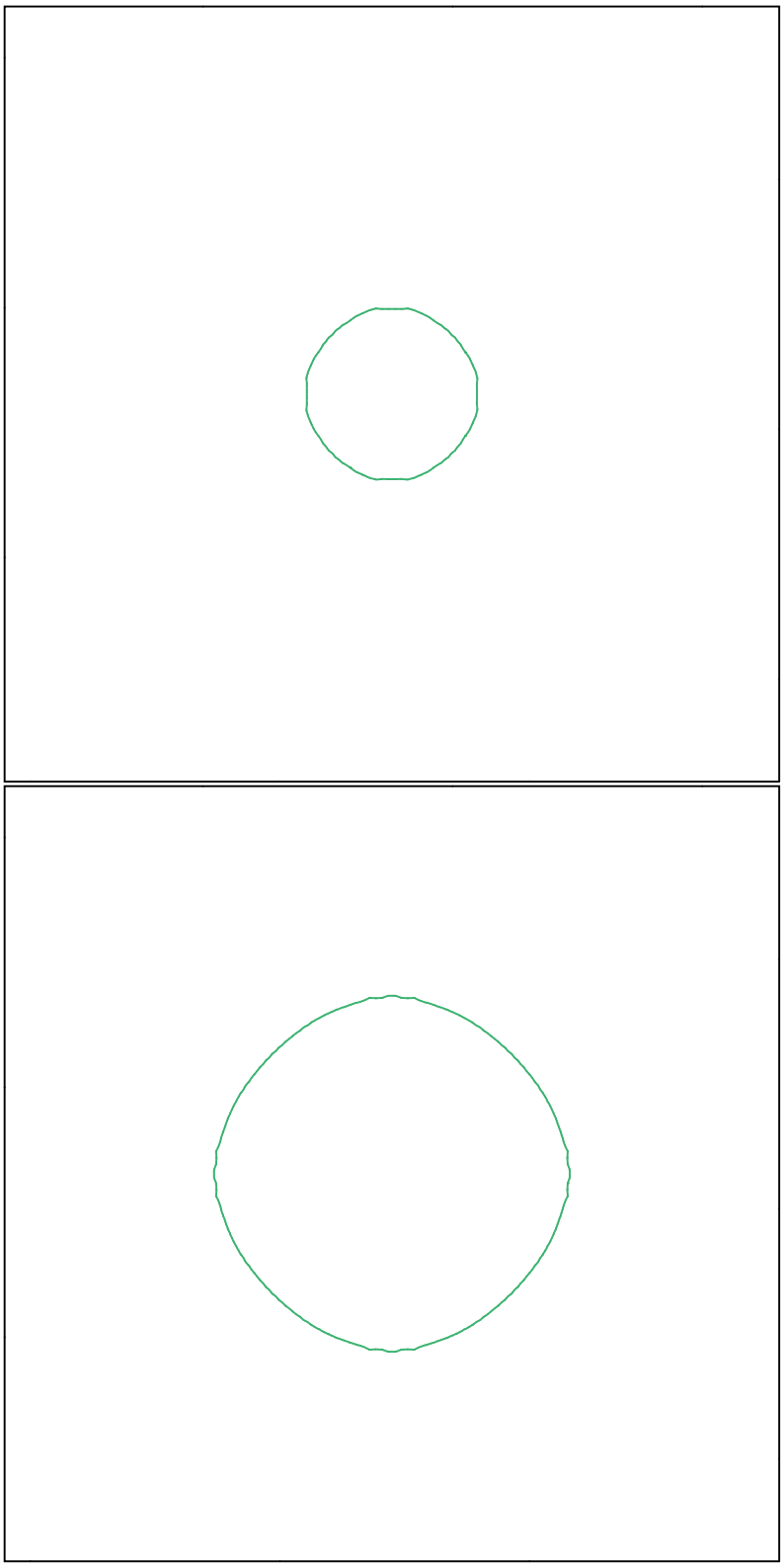

Figure 10: Expansion of a cylindrical high-pressure high-density region. Anti-diffusive approach. α at $t = 1$ (top) and at $t = 10$ (bottom).

In Figure 11 we represent the solution on the cell centers with $y = 0$ (the curvilinear abscissa involving centers begins at $x = 0$ and ends at $x = 120$). As one can see, for the anti-diffusive approach we have only one or two intermediate zones between α equal to 1 and 0. Solution for the anti-diffusive approach with tanh modification is obtained with $\beta = 0.75$. As one can see, at $t = 1$ this solution is as accurate as the one obtained with the Barth-Jespersen approach. At $t = 10$ the number of intermediate regions keeps the same for the former while increase for the latter one, as expected, namely the anti-diffusive approach with tanh modification becomes more accurate than the one involving the Barth-Jespersen reconstruction.

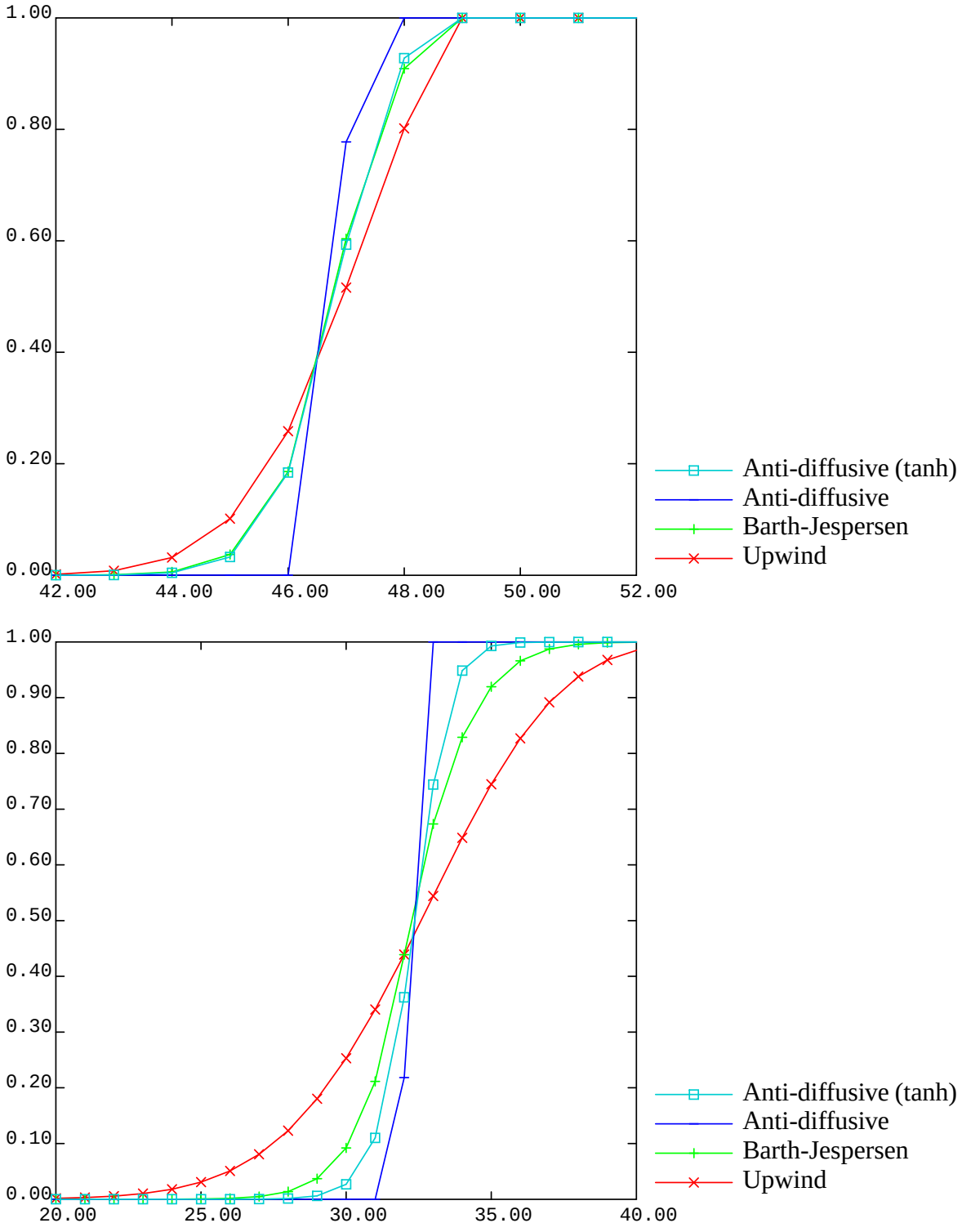

Figure 11: Expansion of a cylindrical high-pressure high-density region. α at $t = 1$ (top) and $t = 10$ (bottom) using different approaches. $y = 0$ (the curvilinear abscissa involving centers begins at $x = 0$ and ends at $x = 120$).

4 Conclusion and perspectives

A modification of the anti-diffusive approach is here proposed in 1D and multi-dimensional cases. This approach uses the hyperbolic tangent function to introduce a space scale for the diffusion region of the color function α. The existence of this diffusion region with a finite width allows a correct computation of gradient of α and then a correct computation of normals to the flame surface. Moreover, as shown by several numerical experiments here considered in reactive and non-reactive cases, the number of intermediate regions (i.e. its width) remains constant in time, making this approach more accurate than the ones which use a classical limited second order reconstruction.

Of course this way of computing normals does not resolve the problem of flame wrinkling, which in the case of the new approach is even more important than in case of approaches involving a limited second order reconstruction (as expected, since numerical diffusion is less important in the former case).

A way of reducing the flame wrinkling is to compute normals to the flame interface using a field obtained by the diffusion of the color function α. If the elimination of the flame wrinkling is a must, further studies should be done in this direction.

REFERENCES

[1] K. Tang, A. Beccantini, and C. Corre, "Combining Discrete Equations Method and upwind downwind-controlled splitting for non-reacting and reacting two-fluid computations," in *Seventh International Conference on Computational Fluid Dynamics (ICCFD7), Big Island, Hawaii, July 9-13*, 2012.

[2] K. Tang, *Combining Discrete Equations Method and Upwind Downwind-Controlled Splitting for Non-Reacting and Reacting Two-Fluid Computations*. PhD thesis, Université de Grenoble, dec 2012.

[3] K. Tang, A. Beccantini, and C. Corre, "Combining Discrete Equations Method and upwind downwind-controlled splitting for non-reacting and reacting two-fluid computations: One dimensional case," *Computers & Fluids*, vol. 93, pp. 74–90, 2014.

[4] K. Tang, A. Beccantini, and C. Corre, "Combining Discrete Equations Method and upwind downwind-controlled splitting for non-reacting and reacting two-fluid computations: Two dimensional case," *Computers & Fluids*, vol. 103, pp. 132–155, 2014.

[5] R. Abgrall and R. Saurel, "Discrete equations for physical and numerical compressible multiphase mixtures," *Journal of Computational Physics*, vol. 186, no. 2, pp. 361–396, 2003.

[6] O. L. Métayer, J. Massoni, R. Saurel, O. Le Métayer, J. Massoni, and R. Saurel, "Modelling evaporation fronts with reactive Riemann solvers," *Journal of Computational Physics*, vol. 205, no. 2, pp. 567–610, 2005.

[7] A. Beccantini and E. Studer, "The reactive Riemann problem for thermally perfect gases at all combustion regimes," *International Journal for Numerical Methods in Fluids*, vol. 64, pp. 269–313, 2010.

[8] "Europlexus, a computer program for the finite element simulation of fluid-structure systems under transient dynamic loading." `http://europlexus.jrc.ec.europa.eu`, visited in October 2015.

[9] E. Studer, A. Beccantini, S. Kudriakov, and A. Velikorodny, "Hydrogen Combustion Modelling in Large-Scale Geometries," in *Volume 6: Beyond Design Basis Events; Student Paper Competition*, p. V006T15A030, ASME, jul 2013.

[10] A. Velikorodny, E. Studer, S. Kudriakov, and A. Beccantini, "Combustion modeling in large scale volumes," in *International Conference on Hydrogen Safety*, (Brussels, Belgium), 2013.

[11] A. Velikorodny, E. Studer, S. Kudriakov, and A. Beccantini, "Combustion modeling in large scale volumes using EUROPLEXUS code," *Journal of Loss Prevention in the Process Industries*, vol. 35, pp. 104–116, may 2015.

[12] F. Xiao, Y. Honma, and T. Kono, "A simple algebraic interface capturing scheme using hyperbolic tangent function," *International Journal for Numerical Methods in Fluids*, vol. 48, pp. 1023–1040, jul 2005.

[13] K. Yokoi, "Efficient implementation of THINC scheme: A simple and practical smoothed VOF algorithm," *Journal of Computational Physics*, vol. 226, no. 2, pp. 1985–2002, 2007.

[14] F. Xiao, S. Ii, and C. Chen, "Revisit to the THINC scheme: A simple algebraic VOF algorithm," *Journal of Computational Physics*, vol. 230, no. 19, pp. 7086–7092, 2011.

[15] S. Ii, K. Sugiyama, S. Takeuchi, S. Takagi, Y. Matsumoto, and F. Xiao, "An interface capturing method with a continuous function: The THINC method with multi-dimensional reconstruction," *Journal of Computational Physics*, vol. 231, no. 5, pp. 2328–2358, 2012.

[16] S. Ii, B. Xie, and F. Xiao, "An interface capturing method with a continuous function: The THINC method on unstructured triangular and tetrahedral meshes," *Journal of Computational Physics*, vol. 259, pp. 260–269, feb 2014.

[17] B. Xie, S. Ii, and F. Xiao, "An efficient and accurate algebraic interface capturing method for unstructured grids in 2 and 3 dimensions: The THINC method with quadratic surface representation," *International Journal for Numerical Methods in Fluids*, vol. 76, pp. 1025–1042, dec 2014.

[18] F. Lagoutière, *Modelisation mathematique et resolution numerique de problemes de fluides compressibles a plusieurs constituants*. PhD thesis, Paris 6, jan 2000.